Hydroformylation of 1-Octene Using [Bmim][PF6]–Decane Biphasic Media and Rhodium Complex Catalyst: Thermodynamic Properties and Kinetic Study

Amit Sharma, Carine Julcour-Lebigue, Raj M. Deshpande, Ashutosh A. Kelkar, Henri Delmas

Hydroformylation of 1-Octene Using [Bmim][PF_6]−Decane Biphasic Media and Rhodium Complex Catalyst: Thermodynamic Properties and Kinetic Study

Amit Sharma,[†,‡] Carine Julcour Lebigue,*[,†,‡] Raj M. Deshpande,[§] Ashutosh A. Kelkar,[§] and Henri Delmas[†,‡]

Université de Toulouse, INP, LGC (Laboratoire de Génie Chimique), 4 allée Emile Monso, BP 84234, 31432 Toulouse Cedex 4, France, CNRS, LGC, 31432 Toulouse Cedex 4, France, and Chemical Engineering and Process Development Division, National Chemical Laboratory, 411008 Pune, India

A chemical reaction engineering approach is reported to investigate the biphasic hydroformylation of 1-octene using [bmim][PF_6] ionic liquid. It is based both on a process parameter investigation (temperature, concentrations, and pressures) and a thermodynamic study of the reaction medium (gas−liquid and liquid−liquid equilibria). Initial rate data show complex behavior with respect to operating parameters and are best described by a rate equation based on a mechanistic model. Complete reaction scheme including isomerization is then modeled accounting from the time dependent concentration of the organic substrates measured in organic phase and recalculated in ionic liquid phase from liquid−liquid equilibria.

1. Introduction

Homogeneous catalysts are used commercially for the synthesis of various bulk and fine chemicals, especially when a high selectivity to desired product is required. However the use of volatile solvents—often environmentally harmful—and the difficulties to separate the products from the reaction media are major drawbacks of homogeneous catalysis. Since the past decade, ionic liquids (ILs) have gained significant importance as alternative solvent systems for catalysis applications. ILs exhibit essential properties that could satisfy the requirements for hydroformylation reaction. First, they have essentially no vapor pressure which avoids problems due to volatility (i.e., safety, losses) faced with conventional organic solvents. Furthermore, they are good solvents for a wide range of both organic and inorganic species without undesirable interactions with the metal center. Moreover their property to be immiscible with a number of organic solvents makes them very promising solvents to substitute for water in the biphasic hydroformylation of olefins.[1]

The first report on the rhodium catalyzed hydroformylation using ionic liquid was proposed by Chauvin et al.:[2] they showed that [$Rh(CO)_2$(acac)]/PPh_3 in [bmim][PF_6] was an efficient catalyst system for the biphasic hydroformylation of 1-pentene. However, the system suffered from catalyst leaching and so various phosphine ligands were investigated. Efficient immobilization of the catalyst in the IL could be achieved with sulfonated ligands (i.e., triphenylphosphine mono- and trisulfonate: TPPMS and TPPTS), but they resulted in lower turn over frequencies (TOFs). Relatively poor selectivity to the desired linear hydroformylation product was also obtained in all cases (*n*/iso ratio between 2 and 4).

Chlorostannate ionic liquids were evaluated by Wasserscheid and Waffenschmidt[3] for the hydroformylation of 1-octene catalyzed by $(PPh_3)_2PtCl_2$. Compared to the monophasic reaction in CH_2Cl_2, activity and *n*/iso ratio were only slightly lower in the biphasic ionic liquid system. However, significant octane was formed which was attributed to a higher solubility of H_2 compared to CO in chlorostannate ionic liquids. Moreover the undesired hydrogenation yield was found to depend significantly on the cation of the ionic liquid (41.7% hydrogenated product with 1-butyl-3-methylimidazolium vs 29.4% with 1-butyl-4-methylpyridinium).

The influence of the nature of the IL on the activity and selectivity of the reaction was further investigated in the works of Favre et al.[4] and Dupont et al.[5]

Favre et al.[4] investigated the [$Rh(CO)_2$(acac)]/TPPTS catalyzed hydroformylation of 1-hexene in eight ionic liquids, varying the nature of the cation (1,3-dialkylimidazoliums) and the anion (e.g., BF_4^-, PF_6^-, $CF_3CO_2^-$, $CF_3SO_3^-$, $N(CF_3SO_2)_2^-$, and NTf_2^-). Except in the case of NTf_2^- based ionic liquids, the observed activity could be well-correlated with the solubility of the substrate in ILs. The *n*/iso ratio was not affected by the nature of the solvent.

Dupont et al.[5] also compared different solvent systems—pure [bmim][PF_6] (hydrophobic), water saturated [bmim][PF_6], [bmim][PF_6] with toluene as cosolvent, and pure [bmim][BF_4] (hydrophilic)—for the hydroformylation of 1-octene. With Rh/sulfonated xantphos complex immobilized in [bmim][PF_6], a very high *n*/iso selectivity (ratio up to 13.1) could be achieved and the catalytic phase could be recycled up to four times without loss in activity. In the hydrophilic or mixed IL systems, lower selectivity to the linear product was observed. This behavior was associated with changes in the structure of the ionic liquids in the presence of the cosolvents, resulting in different miscibilities of alkenes and syngas.

Hydroformylation was also successfully performed in biphasic IL/CO_2 systems.[6−9] Ahosseini et al.[7] reported that the effect of CO_2 pressure on the apparent reaction rate resulting from a complex interplay between the volume expansion of the IL phase, the change in multiphase equilibria, and the modified transport properties.

These few studies have shown that both chemical and thermodynamic aspects have to be considered to evaluate the performances of biphasic IL systems. More examples can be found in the comprehensive review published by Haumann and Riisager.[10]

The use of ionic liquids as solvents to achieve multiphase homogeneous catalysis is explored in the present work following

* To whom correspondence should be addressed. E-mail: carine.julcour@ensiacet.fr.
[†] Université de Toulouse.
[‡] CNRS, LGC.
[§] National Chemical Laboratory.

Table 1. Henry's Constants (H) for H_2 and CO in [bmim][PF_6]

T (K)	H_{H2} (bar·m^3·kmol^{-1})	H_{CO} (bar·m^3·kmol^{-1})
293	898	449
323	816	558
373	869	663

a chemical reaction engineering approach: thermodynamics of multiphase equilibria and reaction kinetics including modeling of the concentration−time profiles of all species. This detailed work is applied to the biphasic hydroformylation of 1-octene using [bmim][PF_6]/decane emulsion and mainly Rh/TPPTS as catalyst. A few experiments have been carried out with sulfoxantphos as a ligand to investigate the influence on activity and selectivity pattern.

2. Solubility Data

As the knowledge of the reactant concentrations in the IL phase is required for the interpretation and modeling of the kinetic data, both gas−liquid and liquid−liquid equilibria were determined for the reaction system.

2.1. Purity of the Ionic Liquid. [bmim][PF_6] 99% was bought from Solvionic. It was delivered with the following specifications: water content less than 0.1% and halide content less than 0.005%. From Karl Fisher titration of the samples, a mean water content of 0.03% was measured. Thermogravimetric analysis (performed at 423 K) showed around 0.15% of volatile compounds. From headspace GC/MS analysis, bromobutane, used for the synthesis of [bmim]$^+$ salt from 1-methylimidazole, was found as the major volatile impurity.

2.2. Solubility of Hydrogen and Carbon Monoxide in [bmim][PF_6]. From the literature, it was observed that the solubility values reported for H_2 and CO varied significantly depending on the experimental methods and ranges of conditions used.[11−16] The variations were as high as 200% under similar conditions. Thus, it was thought necessary to devise a reliable method for determination of solubility of both the gases in [bmim][PF_6]. The measurement technique was based on the batch absorption of a single gas at a given temperature and pressure and measuring of the total gas pressure variation corresponding to the dissolved gas amount in equilibrium with final pressure. More details can be found in our previous article.[17]

Gas solubility was measured at different temperatures (293−373 K) and pressures (up to 25 bar). Both gases follow Henry's law, carbon monoxide being more soluble than hydrogen in the investigated range of temperature. Table 1 gives the corresponding Henry's constants with an estimated uncertainty of less than 5%. At room temperature, these data lie within the range of reported values.[11−16]

As often found in other liquids, the effect of temperature on hydrogen solubility is not monotonous like with other gases and shows a maximum. The solubility of CO and H_2 (per volume of solution) is rather low in [bmim][PF_6] compared to usual organic solvents (around three times lower than in decane at 373 K), but higher than in water.

2.3. Solubility of Olefin and Aldehyde in [bmim][PF_6].
2.3.1. Measurement Techniques. The solubility and partition coefficients of 1-octene and *n*-nonanal in [bmim][PF_6] were much more difficult to measure, as routine chromatography or spectroscopy methods are not suitable. For binary mixtures, IL/1-octene and IL/*n*-nonanal, thermogravimetry analysis (TGA) could be used due to the nonvolatile character of the IL. The TGA unit (TA Instruments SDT Q600) was composed of a precision microbalance with a maximum capacity of 200 mg and a sensitivity of 0.1 μg. Analyses were performed by heating the sample at 423 K under inert atmosphere (nitrogen) and recording the weight loss until no more variation was observed. Prior to the analysis of the saturated sample, a blank measurement was performed on the ionic liquid itself (same lot) to quantify the amount of volatile impurities. This amount was subtracted from the total weight loss recorded with the saturated IL, assuming thus that the impurities were not transferred to the organic phase. Nevertheless this amount of impurities was checked to be much less than the amount of solute for a reliable measurement (not more than 0.15% of the total weight).

Table 2. Solubility of 1-Octene and *n*-Nonanal in [bmim][PF_6] (wt %)

system	T (K)	TGA (wt %)	MHS-GC/MS (wt %)
1-octene/[bmim][PF_6]	298	0.6± 0.05	0.64
	323	0.52	0.59 ± 0.002
	353	0.85 ± 0.2	0.86 ± 0.15
n-nonanal/[bmim][PF_6]	298	11.6 ± 0.5	15.5 ±0.2
	323	10.5	15.3 ± 0.9
	353	11.3 ± 0.3	12.9 ± 0.3

For ternary or quaternary systems, IL/1-octene/decane/*n*-nonanal, a more complex technique was adopted involving multiple headspace gas chromatography (MHS-GC) in which the liquid sample is heated and only the vapor phase is injected in GC and analyzed. The GC-MS apparatus (Trace GC 2000 coupled with PolarisQ detector, ThermoFinnigan) included a CombiPal Automatic Prep & Load Sampler for Headspace (CTC Analytics) with the following features: XYZ robot, syringe heater, shaken incubator oven for equilibrating the sample, and venting tool for headspace pressure release between extractions. A polar capillary column (Varian VF-23 ms, 30 m × 0.25 mm, 0.25 μm film thickness with a stationary phase of cyanopropyl) was used for separation and quantification purpose. The headspace parameters, dilution factor of the sample, sampling volume, and split ratio were set so that the response was high enough for a good sensitivity (but within the linearity domain of the detector) and the extraction of the solute was significant enough (but without depletion before the end of the consecutive headspace sampling steps). A calibration was also made by applying the MHS procedure to standards prepared by dissolving different amounts of 1-octene or *n*-nonanal in [bmim][PF_6] (much below their solubility). The detailed procedure is described elsewhere.[18]

2.3.2. Solubility Results. Solubilities of 1-octene and *n*-nonanal in [bmim][PF_6] were determined at three different temperatures (298, 323, and 353 K) using both TGA and MHS-GC/MS techniques. Table 2 gives the corresponding values with the maximum deviation evaluated from two repetitions of the measurement.

N-nonanal was found to be much more soluble than 1-octene in [bmim][PF_6] due to its polar nature. Solubility values obtained by both techniques showed a very good agreement in case of 1-octene (less soluble), but the deviation was however large for *n*-nonanal (around 30% difference at 298 K). The temperature influence on the solubility was rather low resulting in less than 35% variation for the two compounds in the temperature range investigated (298−353 K). More importantly and as expected, the solubility of 1-octene is significantly higher in [bmim][PF_6] (1.6 mol % at 298 K) than in water (0.0001 mol %), which confirms the potential importance of such solvents for biphasic catalysis. This value is also in accordance with previously reported data (2.0−2.5 mol %[19,20]).

2.3.3. [bmim][PF_6]/Decane Partition Coefficients. In order to estimate partition coefficients of 1-octene and *n*-nonanal in

Table 3. [bmim][PF_6]/Decane Partition Coefficients[a] of 1-Octene and *n*-Nonanal at 353 K, for Different Initial Organic Mixtures

initial organic mixtures (wt %)	partition coefficient of 1-octene (−)	partition coefficient of n-nonanal (−)
mixture 1 (zero conversion; 15% octene + 85% decane)	0.0087 ± 0.002	
mixture 2 (25% conversion; 11.1% octene + 4.7% nonanal + 84.2% decane)	0.0081 ±0.002	0.197 ± 0.03
mixture 3 (50% conversion; 7.4% octene + 9.3% nonanal + 83.3% decane)	0.0071 ±0.0007	0.144 ± 0.01
mixture 4 (75% conversion; 3.65% octene + 13.85% nonanal + 82.5% decane)	0.0161± 0.0008	0.215 ± 0.04
mixture 5 (full conversion; 18.3% nonanal + 81.7% decane)		0.126 ±0.007 from TGA: 0.088 ± 0.015 (3 measurements)

[a] The partition coefficient is defined as the ratio of the weight percent of solute in the IL phase to the weight percent of solute in the organic phase at equilibrium.

the [bmim][PF_6]/decane solvent system, five different organic mixtures were prepared closely matching the concentrations observed during the course of the reaction (Table 3). All measurements were performed twice and analyzed with MHS-GC/MS. Due to the very low solubility of decane (0.13 wt % at 353 K) compared to nonanal, an estimation could also be made from TGA analysis for the last mixture.

Decane has very low solubility in [bmim][PF_6], and hence, the presence of decane does not modify the partitioning of 1-octene or nonanal between organic and IL phases. However, *n*-nonanal seems to enhance the affinity of 1-octene for the IL phase. Partition coefficients estimated were used to evaluate the concentrations of 1-octene and *n*-nonanal in the ionic liquid phase, as required for the modeling of concentration−time profiles (cf. section 4.2).

3. Kinetic Study of Biphasic Hydroformylation

3.1. Experimental Section. 3.1.1. Materials. $Rh(CO)_2(acac)$ was purchased from Sigma-Aldrich. TPPTS (more than 90% purity with <10% oxide) and sulphoxantphos (>98% purity) ligands were prepared at NCL, Pune (India). [bmim][PF_6] with 99% purity was purchased from Solvionic (more detailed information on impurities is given in §2.1.).

Carbon monoxide and hydrogen were supplied by Linde gas s.a.; 1-octene, decane, and GC standards/solvent (*n*-nonanal, anisole/toluene) were purchased from Sigma Aldrich with a purity >98%.

3.1.2. Experimental Procedure. Hydroformylation experiments were carried out in an autoclave reactor equipped with a gas inducing stirrer. The catalyst precursor $Rh(CO)_2(acac)$ and TPPTS as standard ligand were dissolved in [bmim][PF_6] (40 mL) and added to the reactor. Due to the limited solubility of TPPTS in [bmim][PF_6], no excess ligand was used with respect to the expected rhodium triphosphine complex (P/Rh molar ratio of 3 based on pure TPPTS amount). The catalyst complex was synthesized in situ at 80 °C under 20 bar of syngas (3 h). After cooling and releasing the pressure, the reactor was also loaded with the organic phase comprising 1-octene and decane (60 mL). The resulting liquid−liquid system was again pressurized with syngas (10 bar) and heated up to the desired temperature under low stirring (under self-gas induction) to hinder gas−liquid mass transfer. When thermal equilibrium was reached, syngas was introduced up to the desired pressure and the reaction was initiated by increasing the agitation speed to a required value. Initial hydroformylation rate and selectivity toward linear aldehyde were obtained from pressure variations of the reservoir feeding the reactor at constant pressure and gas chromatographic analysis of liquid samples (after 1, 3, and 6 h of reaction), respectively.

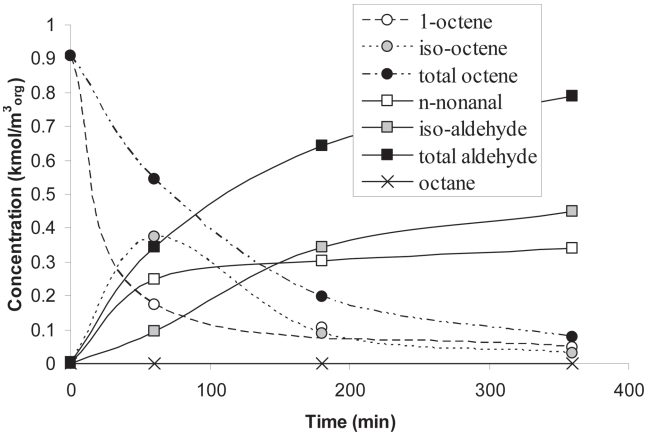

Figure 1. Typical concentration−time profiles for the hydroformylation reaction. Reaction conditions: $Rh(CO)_2(acac)$ 6.97 × 10^{-3} kmol·m_{IL}^{-3}, TPPTS 2.09 × 10^{-2} kmol·m_{IL}^{-3} (P:Rh = 3:1), 1-octene 0.973 kmol·m_{org}^{-3}, *T* 353 K, P_T 40 bar (H_2:CO = 1:1), total liquid volume 100 × 10^{-6} m^3 (organic:IL = 60:40 v/v), agitation speed 1200 rpm.

The organic phase was analyzed using a Varian 3800 gas chromatograph (GC) with a flame ionization detector (FID). A CP Wax 52 column (30 m × 0.32 mm ×0.25 μm film) was used for separation of reactants and products with helium as carrier gas. The quantitative analysis of the products was carried out by means of an internal standard method, using anisole as internal standard and toluene as solvent.

3.1.3. Reaction Parameters. Preliminary experiments were carried out to standardize the reaction and make sure that the data were measured in the kinetic regime. The initial reaction rate was found nearly equal at 1200 and 1500 rpm under standard conditions (see section 3.2.1.). Therefore, all reactions for the kinetic study were carried out at an agitation speed of 1200 rpm high enough to ensure that mass transfer limitation could be ignored.

Following the aforementioned procedure, main reaction parameters were varied: catalyst loading (2.0−7.0 × 10^{-3} kmol·m_{IL}^{-3}), H_2 and CO pressure separately (5−30 bar), 1-octene concentration (0.32−0.97 kmol·m_{org}^{-3}), and temperature (333−353 K). When changing rhodium concentration, the P/Rh ratio was kept constant.

A few experiments were carried out using sulfoxantphos as a ligand (P/Rh = 10) instead of TPPTS to check its influence on the activity and selectivity of hydroformylation.

3.2. Results and Discussion. 3.2.1. Typical Concentration−Time Profiles. Concentration−time profiles of the reactant and products at 353 K is shown in Figure 1 for typical operating conditions (further referred to as standard conditions). It can be observed that the consumption of 1-octene resulted in the formation of both *n*-nonanal and branched aldehydes (three

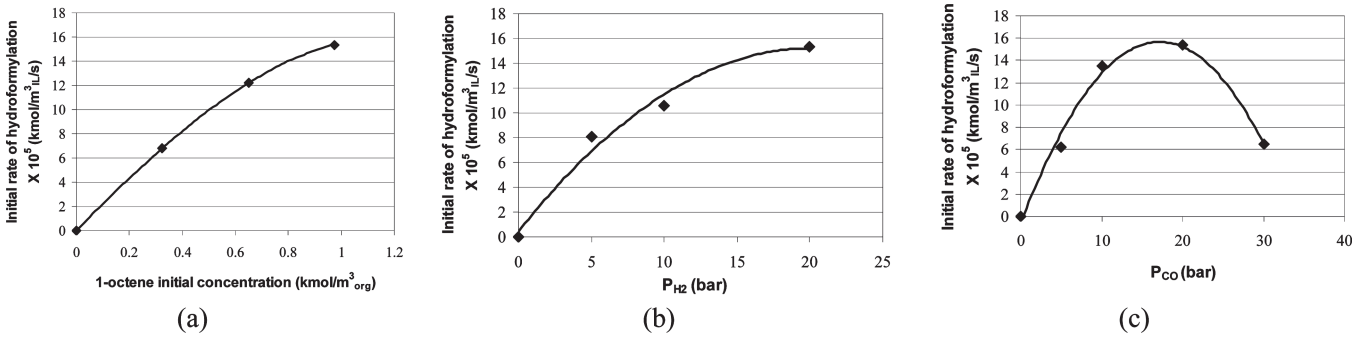

Figure 2. Effect of operating parameters on the initial rate of hydroformylation (other parameters are set according to standard conditions): initial concentration of 1-octene (a), partial pressures of H_2 (b), and CO (c).

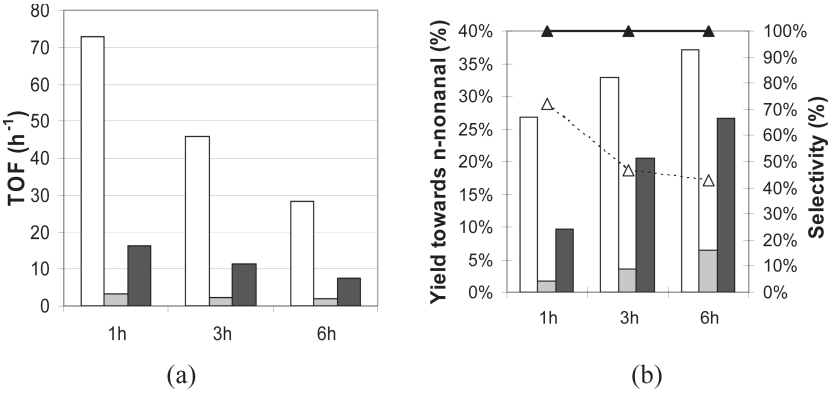

Figure 3. Comparison of TPPTS (white 353 K) and sulphoxantphos (gray 353 K and black 373 K) ligands on the basis of TOF (a), yield (bars), and selectivity (Δ) toward the linear aldehyde (b). yield towards linear aldehyde (%) $= [(n_{n\text{-nonanal}} - n_{n\text{-nonanal},0})/n_{1\text{-octene},0}] \times 100$, selectivity towards linear aldehyde (%) $= (n_{n\text{-nonanal}}/n_{\text{all aldehyde}}) \times 100$. Reaction Conditions: $Rh(CO)_2(acac)$ 6.97×10^{-3} kmol·m_{IL}^{-3}, TPPTS or sulphoxantphos $2.09-3.49 \times 10^{-2}$ kmol·m_{IL}^{-3} (P:Rh = 3:1 or 10:1), 1-octene 0.973 kmol·m_{org}^{-3}, T 353−373 K, P_T = 40 bar (H_2:CO = 1:1), total liquid volume 100×10^{-6} m^3 (organic:IL = 60:40 v/v), agitation speed 1200 rpm.

isomers) as hydroformylation products. All branched aldehydes were clubbed together and termed as "iso-aldehyde". Isomerization of 1-octene was observed as a side reaction, leading to the formation of internal octenes (three isomers), grouped together and termed as "iso-octene". The rate of isomerization of 1-octene was significant during the first hour of reaction; afterward the hydroformylation of iso-octene was predominant. It is noteworthy that *n*-nonanal was formed much faster than iso-aldehyde at the beginning. This result suggests that the direct formation of the branched aldehyde from 1-octene might be rather low. Because of the isomerization reaction, the concentration of iso-octene was maximum after 1 h, leading to formation of iso-aldehyde, which contributed to becoming the major product at the end of the reaction. As a consequence, the *n*/iso ratio decreased as the reaction proceeded, from 2.6 at 1 h to 0.8 at 6 h in the conditions of Figure 1.

As shown in Figure 1, the hydrogenation of 1-octene was found to be negligible. Thus it was verified that the quantity of syngas consumed was consistent with the amount of aldehyde products formed as per the stoichiometry. A material balance in the organic phase was also checked for each experiment during the course of the reaction and was found to be around 95% for all points with respect to the original solution.

3.2.2. Effect of Catalyst Concentration. The effect of $Rh(CO)_2(acac)$ concentration was studied at 353 K, keeping all other parameters constant as per standard reaction conditions. The initial rate of reaction showed first-order dependence on the concentration of the catalyst, proving that all rhodium atoms were working as catalyst at the same TOF and that no mass transfer limitation was present. Plotting of species concentration as a function of time × w_{cat} (where w_{cat} is the weight of $Rh(CO)_2(acac)$) also resulted in similar profiles for the different catalyst loadings (with a maximum of iso-octene found at the same location).

3.2.3. Effect of Initial Concentration of 1-Octene. The initial concentration of 1-octene was varied from 0.325 to 0.973 kmol·m_{org}^{-3} (decreasing the weight percentage of decane in the organic mixture accordingly) while keeping the other parameters the same. The rate of hydroformylation followed a fractional dependence of 0.75 with respect to the olefin concentration (Figure 2a). The variation of TOF was also consistent, showing a quasi linear increase with 1-octene concentration from 30 to 73 h^{-1} after 1 h of reaction. The yield toward *n*-nonanal (38.2%−37.1%) and the *n*/iso aldehyde ratio (0.79−0.76) obtained after the 6 h of reaction remained approximately unaffected by changing the 1-octene concentration.

As per the mechanism proposed by Deshpande et al.[21] for the aqueous biphasic hydroformylation of 1-octene using the Rh/TPPTS complex, an increase in olefin concentration will increase the concentration of acyl complex and hence the rate of the reaction. However, the addition of olefin to catalytic species is an equilibrium reaction and at higher concentrations of olefin the effect of reverse reaction may increase, reducing the apparent order with respect to olefin. Such behavior was observed in homogeneous systems with Rh/PPh_3 catalyst by Bhanage et al.[22] for 1-dodecene hydroformylation and by Kiss et al.[23] for ethene hydroformylation.

3.2.4. Effect of Hydrogen and Carbon Monoxide Partial Pressures. To study the effect of hydrogen and carbon monoxide partial pressures, the cylinder of syngas (H_2:CO = 1:1) was replaced by separate feeds of CO and H_2. Prior to the

Table 4. Rate Models Tested to Fit Experimental Data on Hydroformylation of 1-Octene Using [bmim][PF_6]: Empirical Models (1−8) and Mechanistic Models (9 and 10)[a]

Model 1: $R = \frac{kABCD}{(1 + K_bB)^2}$

Model 2: $R = \frac{kABCD}{(1 + K_bB)^3}$

Model 3: $R = \frac{kABCD}{(1 + K_aA)(1 + K_bB)^2}$

Model 4: $R = \frac{kABCD}{(1 + K_aA)(1 + K_bB)^3}$

Model 5: $R = \frac{kABCD}{(1 + K_aA + K_bB)}$

Model 6: $R = \frac{kABCD}{(1 + K_aA + K_bB)^2}$

Model 7: $R = \frac{kABCD}{(1 + K_aA)(1 + K_bB)^2(1 + K_dD)}$

Model 8: $R = \frac{kABCD}{(1 + K_aA)(1 + K_bB)^3(1 + K_dD)}$

Model 9: $R = \frac{kABCD}{(1 + K_aA + K_bAB + K_cB^2)}$

Model 10: $R = \frac{kABCD}{(1 + K_aB + K_bDB + K_cDB^2 + K_dDB^3)}$

[a] *A*, *B*, *C*, and *D* refer to the concentrations of dissolved H_2, dissolved CO, catalyst, and dissolved olefin in the IL phase, respectively. *R* is the total hydroformylation rate (based on syngas consumption).

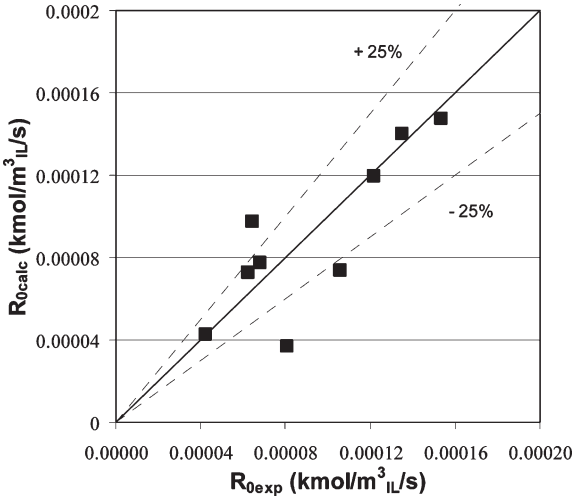

Figure 4. Parity plot of calculated initial rates vs experimental data.

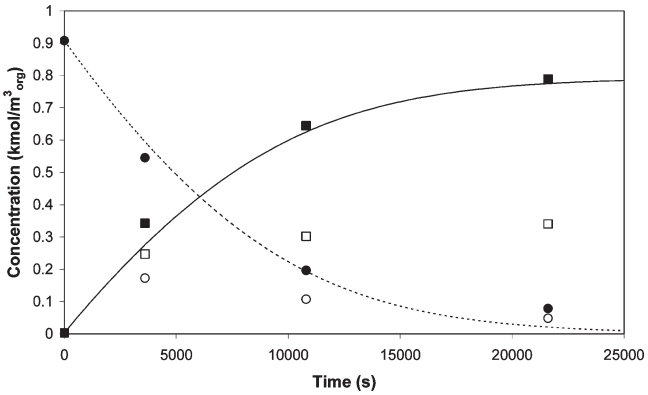

Figure 5. Concentration−time profiles for the main hydroformylation reaction in standard conditions: Experimental: 1-octene (○), total octene (●), *n*-nonanal (□), and total aldehyde (■). Modeling: 1-octene (- - -) and *n*-nonanal (—).

reaction, the ballast was filled up with a selected ratio of H_2:CO so as to feed the reactor to the required total pressure with this gas composition. The ballast was then emptied and filled up with the equimolar mixture of H_2/CO to maintain the desired ratio in the reactor throughout the reaction, as hydrogenation of 1-octene was found negligible. While studying the effect of the partial pressure of a given gas, the partial pressure of the other one was kept constant at 20 bar. Other operating parameters corresponded to standard conditions.

Partial Pressure of H_2. The initial rate of reaction showed fractional order (0.46) with respect to hydrogen partial pressure (Figure 2b). Such a nonlinear effect of H_2 pressure is typical for biphasic hydroformylation and was previously observed by Deshpande et al.[21] and Purwanto and Delmas[24] during the aqueous biphasic hydroformylation of 1-octene using ethanol as a cosolvent. It could be explained by considering that the rate controlling step of the hydroformylation mechanism is the addition of olefin to catalytic species, instead of the well-accepted addition of hydrogen to the acyl complex.[21]

It was also observed that the maximum amount of iso-octene formed was reduced with increasing P_{H2}: while hydroformylation is positively influenced by P_{H2}, the rate of isomerization is not expected to be modified by a change in P_{H2}.

Partial Pressure of CO. The reaction rate first increased with increasing carbon monoxide partial pressure up to about 20 bar and then decreased with further increase in CO pressure, exhibiting a clear maximum (Figure 2c). This observation is again very typical of hydroformylation reactions, observed for both homogeneous and biphasic systems catalyzed by rhodium complex with PPh_3 or TPPTS as ligands. The increase in P_{CO} enhances the CO insertion step of the reaction cycle, but at the same time, it leads to the formation of acyl rhodium di- and tricarbonyl species which are inactive for hydroformylation reaction. Thus, a positive order with respect to CO is only found at low CO pressure while inhibition becomes more and more severe with increasing CO pressure. The location of the maximum at a relatively high CO pressure (∼20 bar) as compared to that observed with ethanol−water mixture[21,24] might be due to the lower solubility of CO in [bmim][PF_6].

As for H_2, the maximum concentration of iso-octene was higher at $P_{CO} = 5$ bar than at $P_{CO} = 20$ bar, CO also having probably no effect on the isomerization rate.

3.2.4. Effect of Temperature. The effect of temperature on the initial rate of hydroformylation was investigated between 333 and 353 K, standard conditions being applied otherwise. As expected, the rate was found to increase with temperature according to the Arrhenius equation. The activation energy was

found to be $E = 107.9$ kJ/mol (25.8 kcal/mol), which is within the range of values observed for hydroformylation reaction.

3.2.5. Effect of Ligand (Sulfoxantphos vs TPPTS). The effect of ligand was studied by testing sulphoxantphos under the same reaction conditions as for TPPTS, but with a higher P/Rh ratio (10 instead of 3) allowed by the better solubility, and at two temperatures: 353 and 373 K. Results are compared on the basis of TOF as well as yield and selectivity toward linear aldehyde in Figure 3a and b, respectively. The reaction using sulphoxantphos ligand led to much lower hydroformylation rates (TOF up to 23 times less than with TPPTS at 353 K), but the selectivity toward *n*-nonanal was much higher as expected from the literature:[5] 100% (no isomers detected) as compared to that of 73% with TPPTS for similar yield toward *n*-nonanal (around 27%).

From the experiments performed at the two temperatures, the activation energy with sulphoxantphos could be roughly estimated at 21.2 kcal/mol, so similar to that obtained with TPPTS.

4. Kinetic Modeling of Biphasic Hydroformylation

4.1. Modeling of Initial Reaction Rates. Rate equations proposed by Deshpande et al.[21] for the aqueous biphasic hydroformylation of 1-octene were considered to model the main reaction kinetics, based on syngas consumption (Table 4). Only the results obtained with TPPTS were considered. The rate models consist of both empirical (models 1−8) and mechanistic models (9−10). All the empirical models (except model 5) describe the inhibition by CO pressure; models 3−5 add the nonlinear effect of H_2 pressure, while models 7 and 8 also account for the nonlinear effect of 1-octene concentration. In models 3−4 and 7−8, the influence of each parameter is described in separate term. Model 9 considers the olefin insertion step as the rate limiting step of the reaction cycle, while model 10 assumes that the addition of hydrogen to the acyl rhodium carbonyl species is the rate determining step.

The concentrations of dissolved CO, H_2, and 1-octene in [bmim][PF_6] required in the kinetic modeling were evaluated from the solubility data reported in section 2.

Detailed optimization work was carried out using Auto2Fit software which allows testing different numerical methods for data regression. The criterion for selecting the best model was based on the sum of squared error (SSE) between the calculated and experimental initial rates:

$$\mathrm{SSE} = \sum_{i=1}^{n} (10^6 R_{0\mathrm{calc},i} - 10^6 R_{0\mathrm{exp},i})^2 \qquad (1)$$

The models were eventually simplified so as to ensure the identifiability of their parameters while keeping same fitting precision.

After a detailed regression and model discrimination procedure, the following equation derived from mechanistic model 10 was found to be the best model to describe the complete reaction runs with 1-octene concentration variation, though it assumes a first order dependence on H_2:

$$R = \frac{kABCD}{(1 + K_\mathrm{d} DB^3)} \qquad (2)$$

with $k = 4064$ (± 1659) (m_{IL}^3/kmol)^3/s and $K_\mathrm{d} = 2\,323\,308$ ($\pm 2\,043\,443$) (m_{IL}^3/kmol)^4.

Figure 4 displays the corresponding parity plot.

4.2. Modeling of Concentration−Time Profiles. 4.2.1. Predictions for Main Hydroformylation Reaction. The aforementioned rate equation (eq 2) was initially applied without further modification to predict the concentration−time profiles of 1-octene and *n*-nonanal under standard conditions assuming no isomerization would occur.

Table 5. Fitted Parameters from Optimization of Concentration−Time Profiles (Series with Different Initial Concentrations of 1-Octene and Catalyst), along with Standard Deviations (Given in Brackets)

k_1 (m_{IL}^3/kmol)^3/s	4396 ($\sigma = 1196$)
K_{d1} (m_{IL}^3/kmol)^4	1.023×10^6 ($\sigma = 1.395 \times 10^6$)
k_2 (m_{IL}^3/kmol)^3/s	3624 ($\sigma = 768.7$)
K_{d2} (m_{IL}^3/kmol)^4	0 ($\sigma = 1.778 \times 10^6$)
k_{io} (m_{IL}^3/kmol)/s	3.947 ($\sigma = 0.2625$)

Table 6. Fitted Parameters from Optimization of Concentration−Time Profiles (Series with Different Initial Concentrations of 1-Octene, Catalyst, and P_{CO}—Except $P_{CO} = 30$ bar), along with Standard Deviations (Given in Brackets)

k_1 (m_{IL}^3/kmol)^3/s	5374 ($\sigma = 913.6$)
K_{d1} (m_{IL}^3/kmol)^4	2.195×10^6 ($\sigma = 1.284 \times 10^6$)
k_2 (m_{IL}^3/kmol)^3/s	2191 ($\sigma = 289.7$)
K_{d2} (m_{IL}^3/kmol)^4	0 ($\sigma = 1.42 \times 10^6$)
k_{io} (m_{IL}^3/kmol)/s	3.693 ($\sigma = 0.2911$)

Corresponding mass balances can be written as follows:

$$\left(V_\mathrm{org} + V_\mathrm{IL} K_\mathrm{woct} \frac{\rho_\mathrm{IL}}{\rho_\mathrm{org}}\right) \frac{\mathrm{d}C_{1\mathrm{oct,org}}}{\mathrm{d}t} = - \frac{k K_\mathrm{woct} \frac{\rho_\mathrm{IL}}{\rho_\mathrm{org}} C_{1\mathrm{oct,org}} C_{\mathrm{H2,IL}} C_{\mathrm{CO,IL}} C_{\mathrm{cat,IL}}}{1 + K_\mathrm{d} C_{\mathrm{CO,IL}}{}^3 K_\mathrm{woct} \frac{\rho_\mathrm{IL}}{\rho_\mathrm{org}} C_{1\mathrm{oct,org}}} V_\mathrm{IL} \qquad (3)$$

$$\left(V_\mathrm{org} + V_\mathrm{IL} K_\mathrm{wnon} \frac{\rho_\mathrm{IL}}{\rho_\mathrm{org}}\right) \frac{\mathrm{d}C_{\mathrm{nnon,org}}}{\mathrm{d}t} = \frac{k K_\mathrm{woct} \frac{\rho_\mathrm{IL}}{\rho_\mathrm{org}} C_{1\mathrm{oct,org}} C_{\mathrm{H2,IL}} C_{\mathrm{CO,IL}} C_{\mathrm{cat,IL}}}{1 + K_\mathrm{d} C_{\mathrm{CO,IL}}{}^3 K_\mathrm{woct} \frac{\rho_\mathrm{IL}}{\rho_\mathrm{org}} C_{1\mathrm{oct,org}}} V_\mathrm{IL} \qquad (4)$$

assuming that both gas−liquid and liquid−liquid equilibria are instantaneous.

These equations were solved using ReactOp Pro software. The likely variation of the partition coefficient of 1-octene with time (as more aldehyde is formed, cf. section 2.3.3.) was not accounted for.

Figure 5 compares these modeled profiles to the experimental data of 1-octene, *n*-nonanal, and lumped alkene and aldehyde species.

The model better matches the experimental profiles of total aldehyde formed and total octene consumed than those of *n*-nonanal and 1-octene respectively, as it was optimized considering the global rate of hydroformylation at time $t = 0$ (based on syngas consumption).

The convenient predictions obtained for these global concentrations throughout the reaction suggest that the model correctly accounts for the dependence of the hydroformylation rate upon 1-octene concentration and that *n*-nonanal and iso-aldehyde should be formed with similar rates.

It can also be noticed that according to the simulation, the material balance in the organic phase is about 90% due to the amount of aldehyde solubilized in the IL phase. It is thus a little bit lower than what is observed experimentally.

4.2.2. Predictions when Accounting for Isomerization. Then a complete model accounting for 1-octene isomerization

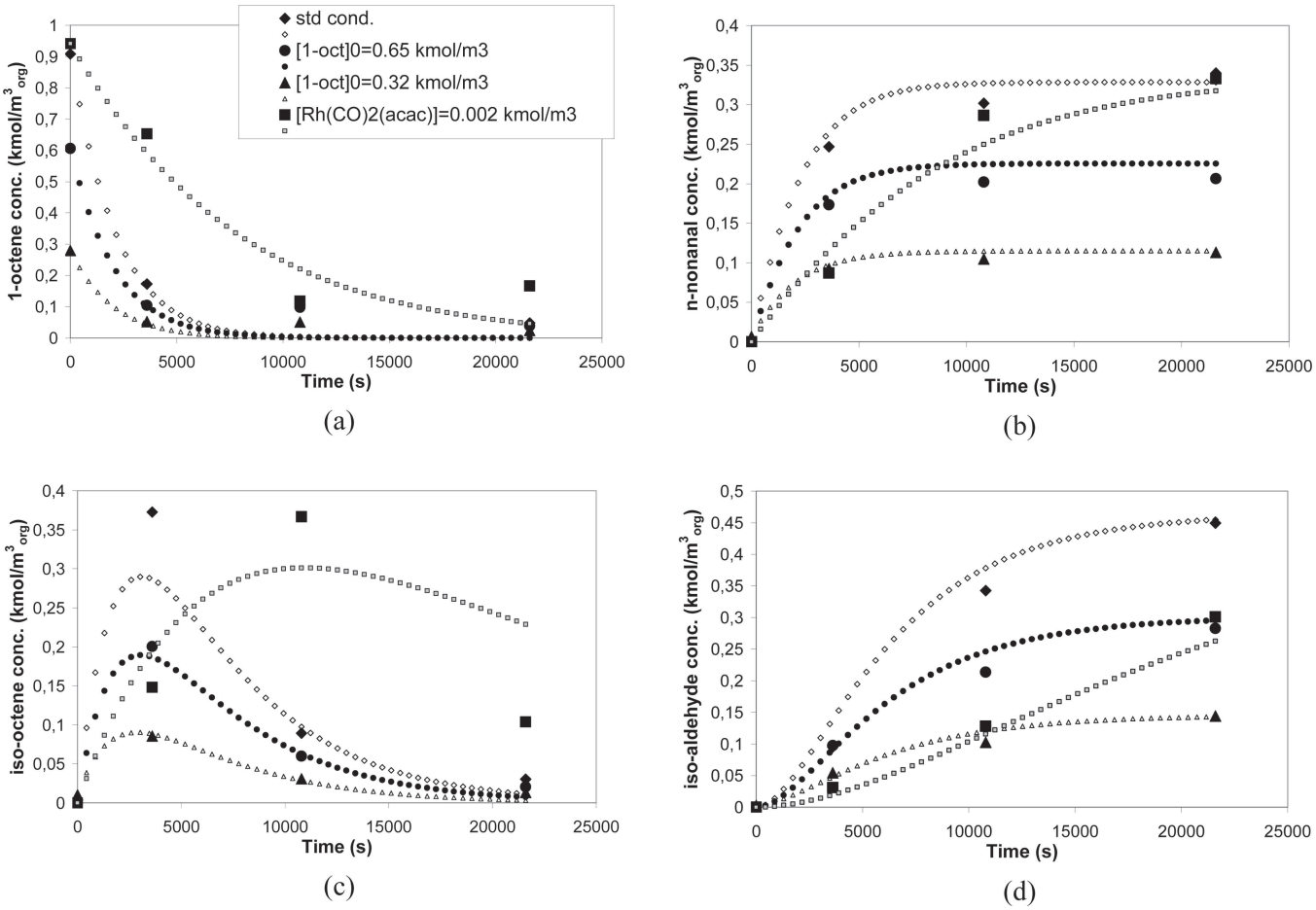

Figure 6. Experimental and predicted concentration−time profiles for the two experimental series considered (parameters of the optimized model are given in Table 5). The legend in part a applies to the entire figure: 1-octene (a), *n*-nonanal (b), iso-octene (c), iso-aldehyde (d).

and hydroformylation of 1- and internal octene was built up considering the following lumped reaction scheme:

$$\text{1-octene} \xrightarrow{R_1} n\text{-nnoanal}$$

$$\text{1-octene} \xrightarrow{R_2} \text{iso-octene}$$

$$\text{iso-octene} \xrightarrow{R_3} \text{iso-aldehyde}$$

It was assumed that the direct formation of iso-aldehyde from 1-octene is negligible. Isomerization was modeled as an irreversible reaction.

Rate equations were written as follows for the two hydroformylation reactions:

$$R_1 = \frac{k_1 K_{\text{woct}} \frac{\rho_{\text{IL}}}{\rho_{\text{org}}} C_{\text{1oct,org}} C_{\text{H2,IL}} C_{\text{CO,IL}} C_{\text{cat,IL}}}{1 + K_{\text{d1}} C_{\text{CO,IL}}{}^3 K_{\text{woct}} \frac{\rho_{\text{IL}}}{\rho_{\text{org}}} C_{\text{1oct,org}}} \quad (5)$$

$$R_3 = \frac{k_2 K_{\text{woct}} \frac{\rho_{\text{IL}}}{\rho_{\text{org}}} C_{\text{ioct,org}} C_{\text{H2,IL}} C_{\text{CO,IL}} C_{\text{cat,IL}}}{1 + K_{\text{d2}} C_{\text{CO,IL}}{}^3 K_{\text{woct}} \frac{\rho_{\text{IL}}}{\rho_{\text{org}}} C_{\text{ioct,org}}} \quad (6)$$

Partition coefficients of octene and aldehyde isomers were supposed to be equal to those of 1-octene and *n*-nonanal, respectively.

The isomerization reaction was assumed to be first order with respect to both catalyst and 1-octene concentrations and independent of hydrogen and carbon monoxide partial pressures:

$$R_2 = k_{\text{io}} K_{\text{woct}} \frac{\rho_{\text{IL}}}{\rho_{\text{org}}} C_{\text{1oct,org}} C_{\text{cat,IL}} \quad (7)$$

Similar mass balances as written in eqs 3 and 4 were applied for the four lumped species (1-octene, internal octene, *n*-nonanal, and branched aldehyde). The kinetic parameters k_1, k_2, K_{d1}, K_{d2}, and k_{io} were optimized with the help of ReactOp Pro software using the time variations of the concentrations measured in organic phase and recalculated in ionic phase with the equilibrium models (cf. eqs 3−7).

Only the experiments for which the initial reaction rate matches with the value given by the rate model were considered for optimization. First, the two series investigating the effects of initial concentration of 1-octene and catalyst concentration were used as database. Corresponding estimated parameters are given in Table 5, and comparison between experimental and predicted profiles is shown in Figure 6.

The concentration−time profiles of all species could be quite well described by the model (cf. Figure 6), but the applied rate model might not be so adequate to describe the hydroformylation of iso-octene (R_3), as the optimization software converged toward the lowest bound of the searching interval for K_{d2} ($K_{\text{d2}} \geq 0$). Actually it was found that the regression criteria and optimized profiles were not much sensitive to the values of K_{d1} and K_{d2} as confirmed by the large standard deviations obtained for those parameters.

When adding data obtained at different P_{CO} (P_{CO} = 5 and 10 bar), the minimum residual was still obtained for $K_{d2} = 0$ (Table 6) and the optimized model showed larger discrepancies with respect to the concentration−time profiles of iso-aldehyde (mean relative deviation increasing from 14 to 51%).

Further work is thus required to better understand the full reaction mechanism. More rate models will have to be tested and probably complementary experiments will also have to be performed (for instance varying simultaneously P_{H2} and P_{CO}). Nevertheless this modeling work is already promising and shows that such chemical engineering approach could also be useful to understand hydroformylation mechanism.

5. Conclusion

The kinetics of biphasic hydroformylation of 1-octene was studied using Rh/TPPTS catalyst and [bmim][PF_6] as a catalyst solvent. The rate of hydroformylation was found to be first-order with respect to catalyst concentration and partial-order with respect to both olefin concentration (0.75) and hydrogen partial pressure (0.43). Its evolution versus CO concentration exhibited a maximum, indicating an inhibition at higher pressures. The activation energy was found to be 25.8 kcal/mol.

The concentrations of dissolved CO, H_2, and 1-octene in [bmim][PF_6] required in the kinetic modeling were evaluated from solubility data obtained experimentally at different temperatures, using the pressure-drop technique for gas−liquid equilibrium and multiple headspace gas chromatography as well as thermogravimetry for liquid−liquid equilibrium. The solubility of all the components was higher in [bmim][PF_6] than in water, especially for 1-octene whose solubility was higher by 4 orders of magnitude. [bmim][PF_6] as a catalyst solvent resulted in a TOF of the same order (15−75 h^{-1} after 1 h) as those observed in biphasic aqueous catalysis with cosolvent for which comparable enhancement of octene solubility could be achieved.[24]

The kinetic data were represented by a simplified rate equation derived from a classical mechanistic model, excepting the observed trend with respect to hydrogen. A first simulation attempt of the concentration−time profiles including isomerization was also proposed.

As the *n*/iso-aldehyde ratio was quite low with this catalytic system (from about 3 to less than 1 in some cases), the sulphoxantphos ligand was tested as well: it resulted into 100% *n*-nonanal selectivity, but with much lower TOF.

For an industrial application, such a reaction engineering approach should be applied to a more efficient reaction medium, whose chemistry will have been first optimized, regarding for instance the choice of convenient ligand for both activity and selectivity and its concentration to achieve stability.

Acknowledgment

The authors express their gratitude to IFCPAR (project 3305-2) for financial support. They thank Marie Morere (CRITT, LGC Toulouse) for establishing MHS/GC-MS analysis method, Christine Rey-Rouch and Luce Bernard (SAP, LGC Toulouse) for standardization of thermogravimetry and liquid−liquid equilibrium measurements, and Jean-Louis Labat and Ignace Coghe (LGC Toulouse) for the setting up and instrumentation of the autoclave.

Notations

$C_{i,x}$ = concentration of i in x phase (kmol/m^3)
H = Henry's constant (bar·m^3/kmol)
k = reaction rate constant as defined by models 1−10 (m_{IL}^3/kmol)^3/s
K_a, K_b, K_c, K_d = constants derived from equilibrium constants as defined by models 1−10
K_{wnon} = partition coefficient of *n*-nonanal between the IL phase and the organic phase at considered equilibrium (kg_{org}/kg_{IL})
K_{woct} = partition coefficient of 1-octene between the IL phase and the organic phase at considered equilibrium (kg_{org}/kg_{IL})
P_{H2} = hydrogen partial pressure (bar)
P_{CO} = carbon monoxide partial pressure (bar)
R = hydroformylation rate (kmol/m_{IL}^3)/s
t = time (s)
T = temperature (K)
TOF = turn over frequency (h^{-1})
V_{IL} = volume of ionic liquid phase (m^3)
V_{org} = volume of organic phase (m^3)
Greek Symbols
ρ = density (kg/m^3)
Subscripts
cat = catalyst
CO = carbon monoxide
H2 = hydrogen
iald = iso-aldehyde
IL = ionic liquid phase
ioct = iso-octene
nnon = *n*-nonanal
1oct = 1-octene
org = organic phase

Literature Cited

(1) Wasserscheid, P; Welton, T. *Ionic liquids in synthesis*; Wiley-VCH: Weinheim, 2003.

(2) Chauvin, Y.; Mussmann, L.; Olivier, H. A novel class of versatile solvents for two-phase catalysis: hydrogenation, isomerization, and hydroformylation of alkenes catalyzed by rhodium complexes in liquid 1,3-dialkylimidazolium salts. *Angew. Chem., Int. Ed.* **1995**, *34* (23−24), 2698.

(3) Wasserscheid, P.; Waffenschmidt, H. Ionic liquids in regioselective platinum-catalysed hydroformylation. *J. Mol. Catal. A* **2000**, *164*, 61.

(4) Favre, F.; Olivier-Bourbigou, H.; Commereuc, D.; Saussine, L. Hydroformylation of 1-hexene with rhodium in non-aqueous ionic liquids: how to design the solvent and the ligand to the reaction. *Chem. Commun.* **2001**, 1360.

(5) Dupont, J.; Silva, S. M.; de Souza, R. F. Mobile phase effects in Rh/sulfonated phosphine/molten salts catalysed the biphasic hydroformylation of heavy olefins. *Catal. Lett.* **2001**, *77* (1−3), 131.

(6) Scurto, A. M.; Leitner, W. Expanding the useful range of ionic liquids: melting point depression of organic salts with carbon dioxide for biphasic catalytic reactions. *Chem. Commun.* **2006**, 3681.

(7) Ahosseini, A.; Ren, W.; Scurto, A. M. Understanding Biphasic Ionic Liquid/CO_2 Systems for Homogeneous Catalysis:Hydroformylation. *Ind. Eng. Chem. Res.* **2009**, *48* (9), 4254.

(8) Sellin, M. F.; Webb, P. B.; Cole-Hamilton, D. J. Continuous flow homogeneous catalysis: hydroformylation of alkenes in supercritical fluid-ionic liquid biphasic mixtures. *Chem. Commun.* **2001**, 781.

(9) Webb, P. B.; Sellin, M. F.; Kunene, T. E.; Williamson, S.; Slawin, A. M. Z.; Cole-Hamilton, D. J. Continuous Flow Hydroformylation of Alkenes in Supercritical Fluid-Ionic Liquid Biphasic Systems. *J. Am. Chem. Soc.* **2003**, *125* (50), 15577.

(10) Haumann, M.; Riisager, A. Hydroformylation in room temperature ionic liquids (RTILs): catalyst and process developments. *Chem. Rev.* **2008**, *108* (4), 1474.

(11) Berger, A.; de Souza, R. F.; Delgado, M. R.; Dupont, J. Ionic liquid-phase asymmetric catalytic hydrogenation: Hydrogen concentration effects on enantioselectivity. *Tetrahedron: Asymm.* **2001**, *12*, 1825.

(12) Dyson, P. J.; Laurenczy, G.; Ohlin, C. A.; Vallance, J.; Welton, T. Determination of hydrogen concentration in ionic liquids and the effect (or lack of) on rates of hydrogenation. *Chem. Commun.* **2003**, 2418.

(13) Ohlin, C. A.; Dyson, P. J.; Laurenczy, G. Carbon monoxide solubility in ionic liquids: determination, prediction and relevance to hydroformylation. *Chem. Commun.* **2004**, 1070.

(14) Kumelan, J.; Perez-Salado Kamps, A.; Tuma, D.; Maurer, G. Solubility of CO in the ionic liquid [bmim][PF_6]. *Fluid Phase Equilib.* **2005**, *228−229*, 207.

(15) Kumelan, J.; Perez-Salado Kamps, A.; Tuma, D.; Maurer, G. Solubility of H_2 in the Ionic Liquid [bmim][PF_6]. *J. Chem. Eng. Data* **2006**, *51* (1), 11.

(16) Jacquemin, J.; Husson, P.; Majer, V.; Costa Gomes, M. F. Low-pressure solubilities and thermodynamics of solvation of eight gases in 1-butyl-3-methylimidazolium hexafluorophosphate. *Fluid Phase Equilib.* **2006**, *240*, 87.

(17) Sharma, A.; Julcour, C.; Kelkar, A. A.; Deshpande, R. M.; Delmas, H. Mass transfer and solubility of CO and H_2 in ionic liquid. Case of [Bmim][PF_6] with gas-inducing stirrer reactor. *Ind. Eng. Chem. Res.* **2009**, *48* (8), 4075.

(18) Sharma, A. Catalytic reaction engineering using ionic liquids. Ph.D. Thesis, INP Toulouse, France, 2009;http://ethesis.inp-toulouse.fr/archive/00000780/.

(19) Stark, A.; Ajam, M.; Green, M.; Raubenheimer, H. G.; Ranwell, A.; Ondruschka, B. Metathesis of 1-Octene in Ionic Liquids and Other Solvents: Effects of Substrate Solubility, Solvent Polarity and Impurities. *Adv. Synth. Catal.* **2006**, *348*, 1934.

(20) Brasse, C. C.; Englert, U.; Salzer, A.; Waffenschmidt, H.; Wasserscheid, P. Ionic Phosphine Ligands with Cobaltocenium Backbone: Novel Ligands for the Highly Selective, Biphasic, Rhodium-Catalyzed Hydroformylation of 1-Octene in Ionic Liquids. *Organometallics* **2000**, *19*, 3818.

(21) Deshpande, R. M.; Purwanto; Delmas, H.; Chaudhari, R. V. Kinetics of Hydroformylation of 1-Octene Using $[Rh(COD)Cl]_2$-TPPTS Complex Catalyst in a Two-Phase System in the Presence of a Cosolvent. *Ind. Eng. Chem. Res.* **1996**, *35*, 3927.

(22) Bhanage, B. M.; Divekar, S. S.; Deshpande, R. M.; Chaudhari, R. V. Kinetics of hydroformylation of 1 -dodecene using homogeneous $HRh(CO)(PPh_3)_3$ catalyst. *J. Mol. Catal. A* **1997**, *115*, 247.

(23) Kiss, G.; Mozelski, E. J.; Nadler, K. C.; VanDriessche, E.; DeRoover, C. Hydroformylation of ethene with triphenylphosphine modified rhodium catalyst: kinetic and mechanistic studies. *J. Mol. Catal. A* **1999**, *138*, 155.

(24) Purwanto, P.; Delmas, H. Gas-liquid-liquid reaction engineering: hydroformylation of 1-octene using a water soluble rhodium complex catalyst. *Catal. Today* **1995**, *24*, 135.